remote sensing

MDPI

Article

Long-Term Variation Study of Fine-Mode Particle Size and Regional Characteristics Using AERONET Data

Juseon Shin [1], Juhyeon Sim [1], Naghmeh Dehkhoda [1], Sohee Joo [1], Taegyeong Kim [1], Gahyeong Kim [1], Detlef Müller [2], Matthias Tesche [3], Sung-Kyun Shin [4], Dongho Shin [5] and Youngmin Noh [1,*]

1 Division of Earth Environmental System Science, Pukyong National University, Busan 48513, Korea
2 University of Hertfordshire, Hertfordshire AL10 9AB, UK
3 Leipzig Institute for Meteorology, Leipzig University, 04103 Leipzig, Germany
4 Divison of Research Planing, Seoul Institute of Technology, Seoul 03909, Korea
5 Fine Dust Research Department, Korea Institute of Energy Research, Daejeon 34129, Korea
* Correspondence: nym@pknu.ac.kr

Abstract: To identify the long-term trend of particle size variation, we analyzed aerosol optical depth (AOD, τ) separated as dust (τ_D) and coarse-(τ_{PC}) and fine-pollution particles (τ_{PF}) depending on emission sources and size. Ångström exponent values are also identified separately as total and fine-mode particles (α_T and α_{PF}). We checked these trends in various ways; (1) first-order linear regression analysis of the annual average values, (2) percent variation using the slope of linear regression method, and (3) a reliability analysis using the Mann–Kendall (MK) test. We selected 17 AERONET sun/sky radiometer sites classified into six regions, i.e., Europe, North Africa, the Middle East, India, Southeast Asia, and Northeast Asia. Although there were regional differences, τ decreased in Europe and Asian regions and increased in the Middle East, India, and North Africa. Values of τ_{PC} and τ_{PF}, show that aerosol loading caused by non-dust aerosols decreased in Europe and Asia and increased in India. In particular, τ_{PF} considerably decreased in Europe and Northeast Asia (95% confidential levels in MK-test), and τ_{PC} decreased in Northeast Asia (Z-values for Seoul and Osaka are -2.955 and -2.306, respectively, statistically significant if $|z| \geq 1.96$). The decrease in τ_{PC} seems to be because of the reduction of primary and anthropogenic emissions from regulation by air quality policies. The meaningful result in this paper is that the particle size became smaller, as seen by values of α_T that decreased by -3.30 to -30.47% in Europe, North Africa, and the Middle East because α_T provides information on the particle size. Particle size on average became smaller over India and Asian regions considered in our study due to the decrease in coarse particles. In particular, an increase of α_{PF} in most areas shows the probability that the average particle size of fine-mode aerosols became smaller in recent years. We presumed the cause of the increase in α_T is because relatively large-sized fine-mode particles were eliminated due to air quality policies.

Keywords: aerosol optical depth; Ångström exponent; annual variation; fine-mode aerosol; AERONET

Citation: Shin, J.; Sim, J.; Dehkhoda, N.; Joo, S.; Kim, T.; Kim, G.; Müller, D.; Tesche, M.; Shin, S.-K.; Shin, D.; et al. Long-Term Variation Study of Fine-Mode Particle Size and Regional Characteristics Using AERONET Data. *Remote Sens.* **2022**, *14*, 4429. https://doi.org/10.3390/rs14184429

Academic Editors: Alexander Kokhanovsky and Dmitry Efremenko

Received: 25 July 2022
Accepted: 22 August 2022
Published: 6 September 2022

1. Introduction

Atmospheric aerosols are associated with air pollution and public health [1–3]. In particular, small aerosol particles are damaging human health [4,5]. The International Agency for Research on Cancer (IARC) classifies aerosol particles as a class 1 carcinogen [6]. The World Health Organization (WHO) is focusing on the number concentration of ultrafine particles [7]. Because of the hazard of particulate matter (PM), governments worldwide are continuously monitoring and controlling the mass concentration of PM [8–15]. Particle size distribution however cannot be inferred from mass concentration observations [16,17]. To understand the change in air pollution caused by PM and its adverse health effects, we need to identify the variations in size of small particles as well as mass concentration.

According to their sources, ambient atmospheric aerosols can be divided into natural and anthropogenic ones. Anthropogenic aerosols are emitted from industry activities,

population growth, and combustion activities. Aerosols are also classified as fine- and coarse-mode particles depending on their size. Coarse-mode particles are related to primary emissions like industrial activities and biomass burning. This type of particle is highly correlated with the change of mass concentration [18,19]. Fine-mode particles are mainly considered as secondary aerosols formed by gaseous precursors, oxidants, and/or changes of meteorological conditions [20–28]. This particle type is closely related to visibility and adverse effects on human health. Liu et al. (2020) stated that secondary aerosols such as $PM_{2.5}$ still cause haze as the result of high pollution levels, despite the fact that aerosol mass concentration levels have decreased in Beijing in recent years.

Many studies show that aerosol mass concentration and aerosol optical depth (AOD, τ) have decreased globally in recent years [9–11,13,15,29,30]. However, these changes vary by region. These parameters provide little information on the optical properties and size distribution of the pollution particles. Plus, we have difficulty confirming the change of fine-mode particles using changes of mass concentration.

This research developed a method to separate τ as dust and coarse-/fine-mode pollution particles using size distribution and the linear depolarization ratio (δ_p). This method was applied to the long-term observation data of the Aerosol Robotic Network (AERONET) sun/sky radiometer [16,31–35] to determine aerosol types. We also analyzed the proportion of fine mode in the total aerosols, particle size characteristics change, and regional characteristics [31,36,37]. We especially concentrated on the overall change in τ of classified aerosols and particle size of total and fine particles.

2. Methodology

2.1. Study Sites

We selected AERONET Sun/sky radiometer sites that meet the following criteria: First, the sites have acquired data continuously for more than nine years since 2001, making them suitable for studying the long-term trend of τ. Second, the depolarization ratio is essential to calculate dust ratio, so regions with high data loss for depolarization ratio, i.e., all American and some European sites, were not available. Third, the selected observation sites need to be representative of regional characteristics.

Eventually, we chose 17 AERONET sites to identify the annual change of regional aerosol particle characteristics. These sites are distributed across six regions, i.e., Europe, North Africa, Middle East, India, Southeast Asia, and Northeast Asia (Figure 1). The stations Venice (Italy, 45.310°N, 12.51°E), Thessaloniki (Greece, 40.63°N, 22.96°E) are located in Europe. Venice is an urbanized and industrial area, having large harbors and power plants [38–41], and an important city that has the most important wetland sites showing human interferences to the ecosystems [42]. Thessaloniki is the second largest city in Greece and populated [43]. We also add Erdemli (Turkey, Institute of Marin Science-Erdemli, 36.56°N, 34.26°E) to the European site as Turkey is bordering the eastern Mediterranean Sea.

There are four sites in Africa. Tamanrasset (Algeria, 22.79°N, 5.53°E) and the Cape Verde (16.73°N, 22.94°W) stations are located in the dust emission belt that stretches from North Africa westward out into the Atlantic Ocean. Cinzana (Mali, 13.28°N, 5.93°W) is located in the northwest part of the Sahel zone and is mainly affected by Saharan dust outbreaks. Ilorin (Nigeria, 8.48°N, 4.67°E) is located at the upper tip of the Guinea savannah zone in the sub-Sahel. This station is mainly influenced by Saharan dust and biomass burning aerosol [44].

There are two measurement sites in the Middle East. i.e., Sede Boker (Israel, 30.86°N, 34.78°E) and Mezaira (the United Arab Emirates, 23.10°N, 53.75°E). The regions in India, i.e., Kanpur (26.51°N, 80.23°E) and Ballia (Gandhi_College, 25.87°N, 84.13°E) are in Uttar Pradesh which is a state in northern India. These sites are influenced mainly by large-scale anthropogenic emission sources (biomass burning, fossil-fuel combustion, and industrial activities) and mineral dust transported from western India [45].

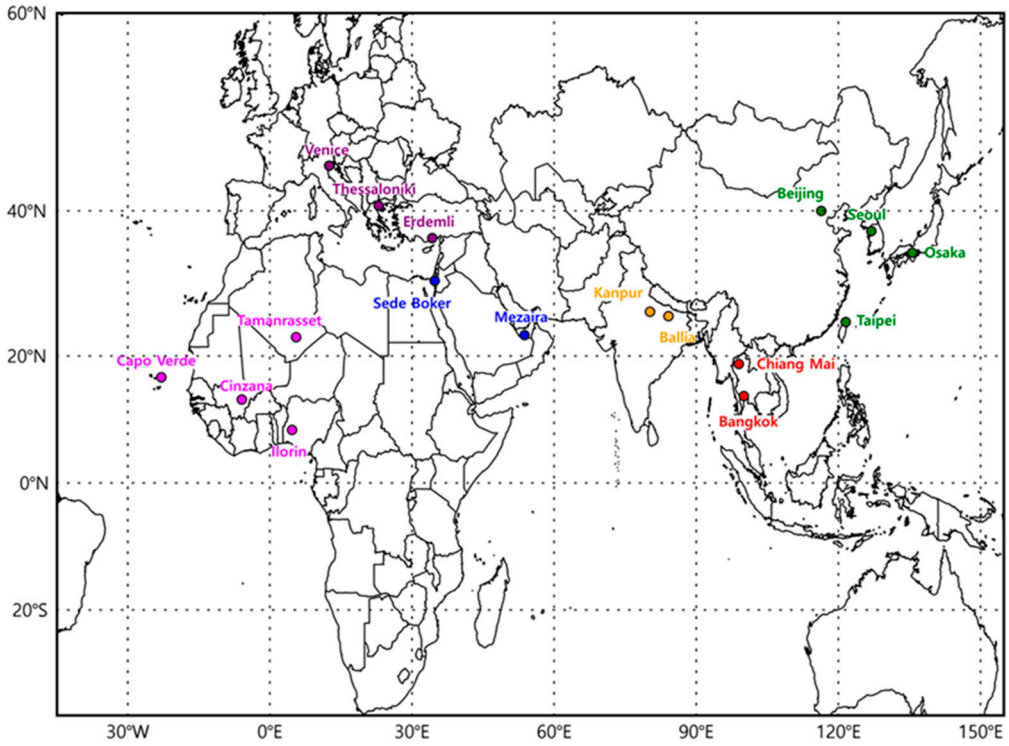

Figure 1. Location of the AERONET Sun/sky radiometer stations considered in our research work. Different colors indicate the regional locations, i.e., purple (Europe), pink (North Africa), blue (the Middle East), yellow (India), red (Southeast Asia), and green (Northeast Asia).

Two Southeast Asia sites, Chiang Mai (18.77°N, 98.97°E) and Bangkok (Silpakorn University, 13.82°N, 100.04°E) are located in northern and central Thailand and have the characteristics of an urban environment. Four sites, Beijing (China, 39.98°N, 116.38°E), Seoul (Korea, 37.46°N, 126.95°E), Osaka (Japan, 34.65°N, 135.59°E), and Taipei (Taiwan, 25.02°N, 121.54°E) are representative regions in Northeast Asia. Beijing is known as the region with the highest concentration of pollution particles worldwide [9]. Seoul is downwind of westerly winds from Beijing and thus often affected by long-range transport of pollution particles from China [46–48]. Seoul also has a high concentration of locally produced pollution particles. Osaka is a coastal city that produces less anthropogenic pollution than China and Korea [46,47]. The effect of long-range transport of pollution on Taipei is relatively low [49].

Northeast Asia and Indian areas are the regions with high levels of aerosol emissions globally; so, we need to observe aerosol properties intensely. All 17 sites provide us with version 3 level 2.0 data for a minimum of 9 years. The total number of observation days per year is shown in Supplementary Table S1.

2.2. AOD Separation into Dust, Coarse- and Fine-Mode Pollution Using Depolarization Ratio

WHO recommended type classification of PM like black carbon or elemental carbon (BC/EC), ultrafine particles (UFP), and particles originating from sand and dust storms (SDS) to manage control of emission of aerosols effectively [7]. Although not explicitly classified based on WHO guidelines, we divided aerosol types as dust, fine- and coarse-mode particles depending on depolarization ratio and particle size data.

Dubovik et al. (2006) introduced kernel look-up tables that describe mixtures of spheroid particles [50]. These kernel look-up tables are used to infer the depolarization ratio (δ_p) of mineral dust observed with AERONET sun/sky radiometer. Details of the AERONET inversion algorithm are given by Dubovik et al. (2006) and Noh et al. (2017) [50,51].

The dust ratio (R_D) was used to estimate the contributions of dust and anthropogenic pollution/biomass burning particles to the total aerosol optical depth (τ_T) of mixed aerosol

plumes under the assumption that both types of aerosol particles are externally mixed [46,52,53]. R_D was retrieved from the particle linear depolarization ratio (δ_p). Noh et al. (2017) have shown that the δ_p derived from Sun/sky radiometer observations at 1020 nm and the lidar-derived δ_p at 532 nm show a comparably high correlation. For that reason, we used the δ_p at 1020 nm to retrieve the dust ratio (R_D). Shimizu et al. (2004) and Tesche et al. (2009) suggested a R_D retrieval method on the basis of [46,52]

$$R_D = \frac{(\delta_p - \delta_2)(1 + \delta_1)}{(\delta_1 - \delta_2)(1 + \delta_p)} \quad (1)$$

The parameters δ_1 and δ_2 denote the δ_p at 1020 nm of pure dust and non-dust particles, respectively, of an external mixture of aerosol particles. The values δ_1 and δ_2 can be empirically determined. We use 0.31 for δ_1 in Europe, North Africa, the Middle East, and India. We use 0.30 for the Southeast and Northeast Asia regions, respectively. Those values were determined by the linear depolarization ratios of Saharan and Asian dust presented in previous research work [17,54,55]. We used 0.02 as the minimum value for δ_2 for non-dust aerosols close to spherical [56]. When δ_p was higher than δ_1 or lower than δ_2, R_D was set to 1 or 0, respectively.

The coarse-mode fraction (CMF) observed at 1020 nm is calculated from the ratio of the coarse-mode AOD to the total (coarse- and fine-mode) AOD. Thus, R_D represents the proportion of AOD for pure dust particles in a mixed aerosol plume, while CMF denotes the ratio of coarse-mode particles to the total particle AOD. Besides, the fine-mode fraction (FMF) is calculated as (1-CMF).

The correlation coefficient (R^2) of the linear regression between CMF and R_D varies from 0.21 to 0.84 for the different observation sites (Figure S1, Supplementary Material). Chiang Mai, Bangkok, and the Taipei sites show low R^2 values of 0.34, 0.21, and 0.33, respectively. Since those sites are not located in the main transport route of Asian dust, the influence of dust particles is comparably weak compared to the other sites. The tendency for R_D to increase as CMF increases appears in all sites despite the weak correlation we find in our study.

Most of the dust particles are coarse-mode particles, which means that the value of CMF increases with R_D. CMF is higher than R_D in most cases, which implies that these coarse-mode particles include dust and pollution particles generated by physical and chemical reactions, e.g., coagulation, condensation processes, and hygroscopic growth [51]. The ratio of coarse-mode particles (CMP) denotes the proportion (number concentration) of coarse-mode pollution particles to total particles. Here, dust particles are not considered. This ratio can be calculated by subtracting R_D from CMF at 1020 nm.

$$\mathrm{CMP}_{1020} = \mathrm{CMF}_{1020} - R_D \quad (2)$$

If R_D is higher than CMF, CMP is set to 0.

AOD of dust particles (τ_D) at 1020 nm was calculated with Equation (3) and the use of R_D and S_d.

$$\tau_{D,1020} = \tau_{1020} \times R_D \times \frac{S_{d,1020}}{S_{1020}} \quad (3)$$

Here, 1020 denotes the wavelength at 1020 nm. The parameter S is the lidar ratio of the aerosol mixture. S can be calculated from the AERONET data products. The S_d is the lidar ratio of pure dust particles. It varies in dependence on the desert source. We take the value of 44 and 54 sr at 1020 nm for Asian dust and Saharan dust, respectively [55].

The AOD of coarse-mode pollution particles (τ_{PC}) observed at 1020 nm was calculated by Equation (4). τ_{PC} at 440, 675, and 870 nm was retrieved by Equation (5), i.e.,

$$\tau_{PC,1020} = \tau_{1020}(\mathrm{CMP}_{1020}) \quad (4)$$

$$\tau_{PC,\lambda} = \tau_{PC,1020}\left(\frac{1020}{\lambda}\right)^{\alpha_{PC}} \quad (5)$$

The term α_{PC} is the Ångström exponent of coarse-mode pollution. We used the value of 0.16 and 0.14 for Asian and Saharan dust, respectively [55].

We used Equation (6) to calculate the AOD of the fine-mode pollution (τ_{PF}) contribution

$$\tau_{PF,\lambda} = \tau_{\lambda} - \tau_{D,\lambda} - \tau_{PC,\lambda} \quad (6)$$

2.3. Annual Trend Analysis via Linear Regression Analysis and MK-Test

To identify annual variation trends and regional properties, we calculated the change of τ with three methods. First, we used linear regression analysis on the time series of annual average τ, and we checked the slope and percent variation from 2001 to 2018. Second, we used the linear regression equation y = ax + b, where x is the time (year), and y is the annual average of τ. The slope a describes the change of τ; b is the intercept. The percent variation was calculated from the equation

$$V(\%) = \left(\frac{aN}{\overline{\tau}}\right) \times 100 \quad (7)$$

where $\overline{\tau}$ is the average of τ, N is the number of year, and a is the slope obtained from the linear regression analysis. The *p*-value (probability value) is a scalar that describes how likely the data occurred by random chance. The *p*-value should be small enough, generally lower than 0.05, depending on the level of confidence. We calculated all data and found some statistically significant trends.

We also applied the non-parametric Mann–Kendall (MK) statistical test [57,58] and Sen's slope values to find annual trend and variation [59,60]. The MK-test provides reliable information on the significance of monotonic trends of data in a time series. The Sen's slope explained the magnitude of the trend. Statistics S is calculated by the equation below.

$$S = \sum_{i=1}^{n-1} \sum_{j=i+1}^{n} \mathrm{sgn}(X_j - X_i) \quad (8)$$

where X is data values, i and j are the indices, sgn is + or − sign of the $(X_j - X_i)$, and n represents data points. The value of sgn and variance of S are described by

$$\mathrm{sgn}(X_j - X_i) = \begin{cases} 1 & if\ X_j - X_i > 0 \\ 0 & if\ X_j - X_i = 0 \\ -1 & if\ X_j - X_i < 0 \end{cases} \quad (9)$$

$$V(S) = \frac{1}{18}\left[n(n-1)(2n+5) - \sum_{p=1}^{q} t_p(t_p-1)(2t_p+5)\right] \quad (10)$$

Here, q is the number of tied groups and t_p is the data number in p-th group. The statistics z is calculated as follows:

$$Z = \begin{cases} \frac{S-1}{\sqrt{V(S)}} & if\ S > 0 \\ 0 & if\ S = 0 \\ \frac{S+1}{\sqrt{V(S)}} & if\ S < 0 \end{cases} \quad (11)$$

There are two hypotheses on the MK-test. Hypotheses are decided by the significance of the value of Z, which is related to the *p*-value. The following relationships are used:

H_0: null hypothesis (no trend),

H_1: alternative hypothesis (clear trend),

Critical value:

$$|Z| < 1.96\ Accept\ H_0\ (95\%\ Confidence\ level),$$

$$|Z| < 1.65\ Accept\ H_0\ (90\%\ Confidence\ level).$$

Otherwise,

$$|Z| > 1.96\ Accept\ H_1\ (95\%\ Confidence\ level),$$

$$|Z| > 1.65\ Accept\ H_1\ (90\%\ Confidence\ level).$$

The sign of Z indicates an increase (+) or decrease (−). The Z value is generally accepted at a 95% confidence level, but the values and number of analysis elements are too small, so we used confidence levels up to 90% instead.

3. Results and Discussion

3.1. Aerosol-Type Classification

In preparation for separating AOD according to dust-only and coarse- and fine-mode pollution AOD, we carried out an aerosol-type classification to understand the main aerosol types of each selected site. Shin et al., 2019 suggested a new aerosol type classification method [56]. The authors proposed considering (a) the contribution of mineral dust to the aerosol mixture based on a threshold value, denoted as R_D, which could be obtained from the depolarization ratio, in combination with (b) the use of the single-scattering albedo (SSA). This latter parameter allows for identifying absorption properties of pollution/biomass burning aerosols and thus separating this aerosol type from mineral dust. In this study, we used seven aerosol types based on the values of δ_p (see Shin et al., 2019). Aerosols were classified as pure dust (PD, $R_D > 0.89$), dust-dominated mixture (DDM, $0.53 \leq R_D \leq 0.89$), pollution-dominated mixture (PDM, $0.17 \leq R_D < 0.53$), and pollution particles ($R_D < 0.17$). Particles are classified on the basis of SSA as non-absorbing (NA, SSA > 0.95), weakly-absorbing (WA, 0.90 < SSA ≤ 0.95), moderately absorbing (MA, 0.85 ≤ SSA ≤ 0.90), and strongly absorbing (SA, SSA < 0.85) pollution.

Figure 2 shows the annual changes of major aerosol types at the 17 sites from 2001 to 2018. The results of our aerosol classification reflect the regional characteristics of the six regions. In Europe, Southeast Asia, and Northeast Asia, pollution particles are the main type of aerosols. In the Middle East and North Africa, pure dust is dominant. The ratio of NA and WA is high but decreases in the order of Venice, Thessaloniki, and Erdemli. These regions have low values of PDM and DDM ratios, respectively. With regard to the North African region, the Sahara Desert obviously is the predominant source region. Naturally, PD is the predominant aerosol type. Ilorin in the Savannah region of Africa has a higher ratio of SA than other African regions as a result of biomass-burning aerosols. Sede Boker and Mezaira, which are located on the Arabian Peninsula, also show PD and DDM as the major aerosol types. The aerosol types of MA and WA can also be observed in Ilorin. The aerosol types MA and SA appear in Sede Boker and Mezaira but are not as dominant as dust. Thus, anthropogenic pollutants at Ilorin are higher than in the other African regions investigated in our study. Logothetis et al., 2020 reported that coarse-mode absorbing aerosols are dominant in North Africa and the Arabian Peninsula because of dust transported from the Saharan and the Arabian deserts [61]. However, fine-mode particles emitted from human activity in the Arabian Peninsula are also observed in autumn and winter.

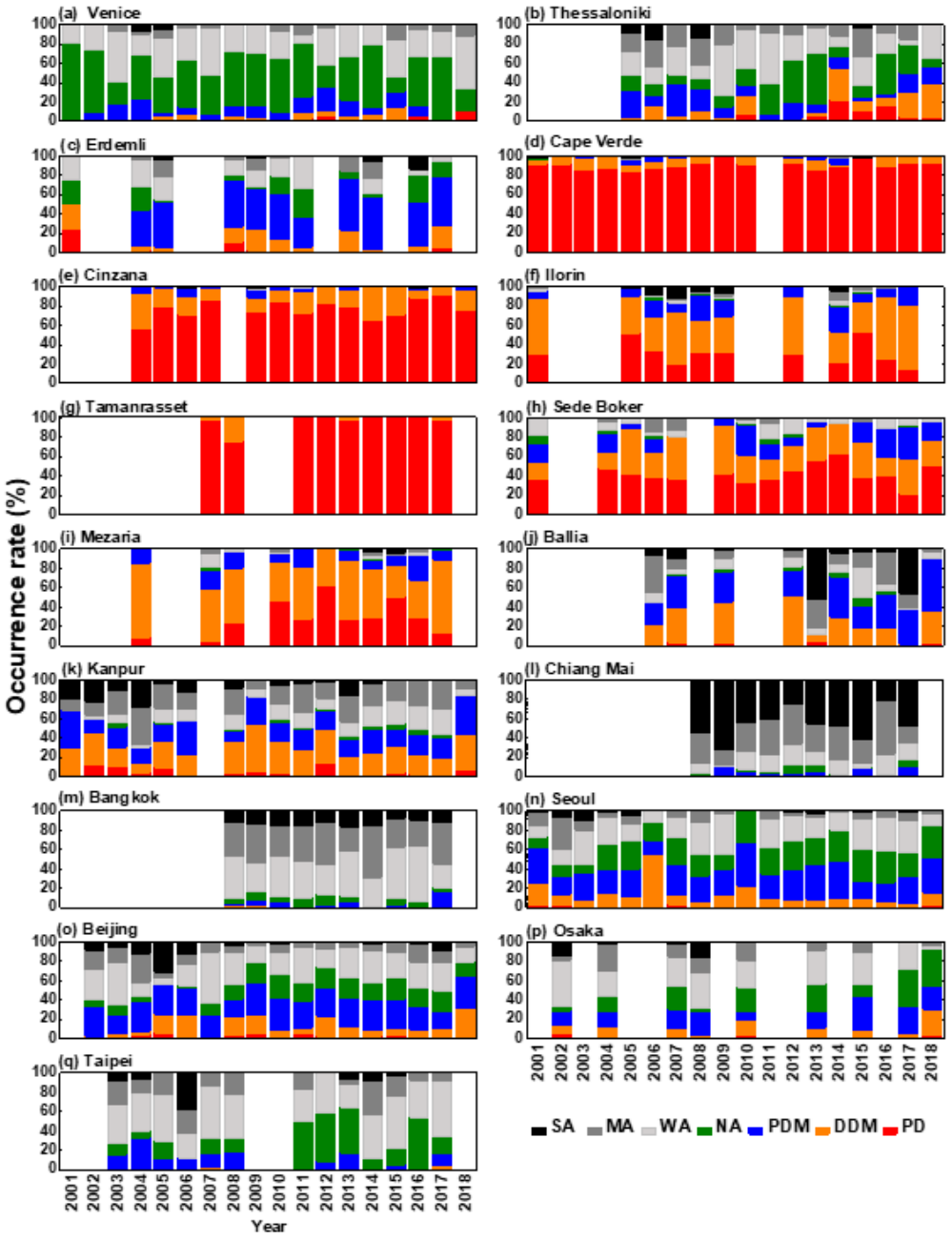

Figure 2. Aerosol type classification expressed in terms of PD (pure dust), DDM (dust dominant mixture), PDM (pollution dominant mixture), and pollution aerosols, and classified in terms of NA (non-absorbing), WA (weakly absorbing), MA (moderately absorbing), and SA (strongly absorbing).

The ratio of dust and pollution particles at Kanpur and Ballia in northern India are similar. Chiang Mai and Bangkok, located in the Indochina Peninsular, are affected mainly by man-made pollution aerosols. The contribution from dust is comparably low. We find 5% for PDM at most. However, these two regions have differences in that the predominant aerosol types over Chiang Mai and Bangkok are SA and WA, respectively. The high value of SA at Chiang Mai is due to biomass burning aerosols emitted by agricultural burning and forest clearing activities during the dry season which lasts from November to April [62]. Bangkok has a low average SSA value of 0.90, but the SA ratio is lower than that of Chiang Mai because the impact of biomass burning is lower [63].

The Northeast Asian region seems to be affected by both dust and pollution [15,22,26,46,47,64,65]. Asian dust heavily affects the Northeast Asian region in spring, i.e., March, April, and May [65]. The ratio of DDM and PDM is high in Beijing which is comparably

close to the source regions of Asian dust. Seoul is located downwind of the emission regions. The impact of dust is relatively low in Osaka, which is relatively far from the source region. Besides, the Osaka site is less affected by Asian dust than the western part of Japan [47]. Shin et al., 2015 stated that dust might mix with pollution when the dust is transported near the surface for a long time [64]. Taipei has the lowest dust effect because it is not located on the pathway of Asian dust.

3.2. Annual Trend of Dust, Coarse- and Fine-Mode Pollution AOD

One aim of our study is to learn more about how AOD may depend on aerosol particle size. Thus, we separated AOD into the contribution by dust-only (τ_D), coarse-mode pollution (τ_{PC}), and fine-mode pollution (τ_{PF}). We used R_D, CMF, and the relationships of Equations (1)–(6). Then, we investigated the change of annual mean values and the regional differences.

Before separating AODs according to aerosol types, we compared trends in the average values of τ_T for each region and site during 2001–2018 (Supplementary Figure S2). The average value of τ_T at 440 nm was highest (1.22 ± 0.76) in Beijing and was lowest (0.48 ± 0.12) in Thessaloniki. Regionally, Northeast Asia (1.22–0.58), Southeast Asia (0.93–0.76), and India (0.82–0.80) show high τ_T values. Europe (0.54–0.48) and the Middle East (0.56–0.49) show low values. The average τ_T value of North Africa except Ilorin (1.04 ± 0.48) tends to be at the lower end of values (Table 1).

Table 1. Average and standard deviation of aerosol optical depth of total (τ_T), dust (τ_D), coarse-mode particles (τ_{PC}) and fine-mode particles (τ_{PF}) at 440 nm, and Ångström exponent (440–870 nm) of total (α_T) and fine-mode particles (α_{PF}), and fine-mode fraction (FMF) for the period 2001–2018.

Site	τ_T (440 nm)	τ_D (440 nm)	τ_{PC} (440 nm)	τ_{PF} (440 nm)	α_T (440–870 nm)	α_{PF} (440–870 nm)	FMF
Thessaloniki	0.48 ± 0.12	0.04 ± 0.08	0.04 ± 0.02	0.42 ± 0.14	1.49 ± 0.42	1.99 ± 0.23	0.91 ± 0.19
Venice	0.54 ± 0.22	0.02 ± 0.05	0.02 ± 0.02	0.51 ± 0.22	1.51 ± 0.28	1.77 ± 0.27	0.96 ± 0.14
Erdemli	0.51 ± 0.13	0.06 ± 0.10	0.06 ± 0.04	0.40 ± 0.12	1.23 ± 0.37	1.90 ± 0.19	0.87 ± 0.18
Cape Verde	0.62 ± 0.25	0.41 ± 0.21	0.12 ± 0.05	0.19 ± 0.08	0.19 ± 0.16	1.56 ± 0.25	0.35 ± 0.15
Cinzana	0.69 ± 0.34	0.46 ± 0.30	0.10 ± 0.07	0.23 ± 0.11	0.27 ± 0.21	1.63 ± 0.24	0.36 ± 0.18
Ilorin	1.04 ± 0.48	0.40 ± 0.30	0.20 ± 0.14	0.51 ± 0.23	0.60 ± 0.31	1.90 ± 0.22	0.61 ± 0.20
Tamanrasset	0.69 ± 0.36	0.53 ± 0.35	0.11 ± 0.06	0.17 ± 0.07	0.13 ± 0.09	1.59 ± 0.20	0.27 ± 0.15
Sede Boker	0.49 ± 0.20	0.23 ± 0.22	0.08 ± 0.05	0.22 ± 0.09	0.57 ± 0.43	1.78 ± 0.27	0.56 ± 0.28
Mezaira	0.56 ± 0.21	0.28 ± 0.23	0.09 ± 0.05	0.26 ± 0.10	0.54 ± 0.35	1.85 ± 0.19	0.53 ± 0.25
Ballia	0.82 ± 0.31	0.13 ± 0.14	0.11 ± 0.07	0.61 ± 0.31	1.01 ± 0.34	1.83 ± 0.23	0.82 ± 0.19
Kanpur	0.80 ± 0.34	0.13 ± 0.19	0.10 ± 0.06	0.60 ± 0.37	0.99 ± 0.39	1.76 ± 0.27	0.82 ± 0.23
Chiang Mai	0.93 ± 0.54	0.01 ± 0.02	0.05 ± 0.04	0.88 ± 0.53	1.57 ± 0.19	1.81 ± 0.20	0.98 ± 0.11
Bangkok	0.76 ± 0.33	0.01 ± 0.02	0.04 ± 0.02	0.71 ± 0.32	1.49 ± 0.19	1.74 ± 0.21	0.98 ± 0.10
Beijing	1.22 ± 0.76	0.08 ± 0.16	0.10 ± 0.07	1.06 ± 0.76	1.14 ± 0.31	1.63 ± 0.31	0.90 ± 0.18
Seoul	0.73 ± 0.37	0.05 ± 0.08	0.04 ± 0.04	0.65 ± 0.37	1.26 ± 0.29	1.68 ± 0.28	0.92 ± 0.15
Osaka	0.58 ± 0.21	0.04 ± 0.08	0.04 ± 0.02	0.51 ± 0.21	1.36 ± 0.31	1.81 ± 0.22	0.92 ± 0.14
Taipei	0.69 ± 0.30	0.01 ± 0.03	0.04 ± 0.02	0.64 ± 0.30	1.34 ± 0.20	1.59 ± 0.24	0.98 ± 0.09

The remarkable thing is the change of the annual averages of τ_T. This change is summarized for each site in Table 2. The values of τ_T decreased every year in Northeast Asia and Europe. Notably, Beijing showed the most prominent decreasing trend of τ_T. We find an average value of $-0.0138\ \tau_T yr^{-1}$. The τ_T in Chiang Mai and Bangkok sites in Southeast Asia also slightly decreased ($-0.0039\ \tau_T yr^{-1}$ and $-0.0012\ \tau_T yr^{-1}$, respectively). However, this decrease of τ_T showed considerable change depending on the years considered in our study. We find, for example, that τ_T was slightly higher from 2008 to 2016 ($0.00117\ \tau_T yr^{-1}$ for Chiang Mai and $0.0107\ \tau_T yr^{-1}$ for Bangkok) and then sharply decreased in 2017 (Figure S2e).

Table 2. Change of the annual value (τyr^{-1} or yr^{-1}) and the percent variation (%) of τ_T, τ_D, τ_{PC}, τ_{PF}, FMF, α_T and α_{PF} based on the slope obtained from linear regression method. The wavelength of τ_T, τ_D, τ_{PC}, and τ_{PF} is 440 nm and that of α_T and α_{PF} ranges from 440 nm to 870 nm.

Region	Site	τ_T (% Variation)	τ_D (% Variation)	τ_{PC} (% Variation)	τ_{PF} (% Variation)	FMF (% Variation)	α_T (% Variation)	α_{PF} (% Variation)
Europe	Thessaloniki	−0.0055 (−17.63)	0.0037 (112.29)	0.0003 (11.94)	−0.0084 (−28.93)	−0.0111 (−18.22)	−0.0155 (−14.92)	0.0073 (5.14)
	Venice	−0.0087 (−29.50)	0.0012 (125.22)	0.0000 (0.00)	−0.0096 (−35.01)	−0.0032 (−6.21)	−0.0040 (−4.78)	0.0015 (1.52)
	Erdemli	0.0010 (2.15)	0.0010 (17.24)	−0.0002 (−3.49)	0.0005 (1.23)	−0.0029 (−15.62)	−0.0055 (−4.45)	−0.0060 (−3.19)
North Africa	Cape Verde	0.0011 (2.78)	0.0002 (0.77)	0.0021 (28.71)	−0.0018 (−15.33)	−0.0025 (−11.39)	−0.0004 (−3.46)	0.0101 (9.51)
	Cinzana	−0.0006 (−1.31)	0.0008 (2.64)	0.0004 (5.80)	−0.0019 (−12.64)	−0.0018 (−4.06)	−0.0030 (−16.82)	0.0052 (4.75)
	Ilorin	0.0006 (0.63)	−0.0001 (−0.27)	−0.0015 (−8.37)	0.0024 (5.19)	0.0025 (9.36)	0.0046 (8.67)	0.0093 (5.43)
	Tamanrasset	0.0108 (13.99)	0.0133 (22.47)	0.0001 (0.83)	0.0001 (0.54)	−0.0030 (−3.74)	−0.0035 (−24.11)	0.0015 (0.85)
Middle East	Sede Boker	0.0020 (6.11)	0.0020 (12.33)	−0.0004 (−7.12)	0.0008 (5.45)	−0.0017 (−5.35)	−0.0012 (−3.30)	0.0052 (4.42)
	Mezaira	0.0049 (9.62)	0.0085 (34.15)	−0.0001 (−1.29)	−0.0014 (−5.76)	−0.0093 (−21.15)	−0.0157 (−30.47)	−0.0119 (−7.08)
India	Ballia	0.0048 (5.79)	−0.0022 (−19.67)	0.0011 (10.53)	0.0055 (9.24)	0.0046 (6.40)	0.0050 (4.93)	−0.0047 (−2.59)
	Kanpur	0.0069 (14.69)	−0.0018 (−23.47)	0.0002 (3.46)	0.0019 (5.39)	0.0032 (7.27)	0.0024 (4.08)	0.0031 (3.02)
Southeast Asia	Chiang Mai	−0.0039 (−4.11)	0.0000 (0.00)	−0.0000 (−0.00)	−0.0039 (−4.36)	−0.0022 (−0.91)	0.0105 (6.68)	0.0163 (8.99)
	Bangkok	−0.0012 (−1.57)	0.0000 (0.00)	−0.0000 (−0.00)	−0.0018 (−2.52)	−0.0002 (−0.08)	0.0119 (8.03)	0.0175 (10.03)
Northeast Asia	Beijing	−0.0138 (−18.10)	0.0011 (22.52)	−0.0005 (−8.21)	−0.0142 (−21.43)	−0.0023 (−4.65)	0.0014 (1.96)	0.0122 (11.92)
	Seoul	−0.0034 (−8.14)	−0.0017 (−56.03)	−0.0010 (−37.81)	−0.0011 (−2.95)	0.0032 (5.91)	0.0095 (13.94)	0.0024 (2.57)
	Osaka	−0.0096 (−14.94)	−0.0008 (−17.57)	−0.0008 (−18.37)	−0.0090 (−15.99)	−0.0020 (−2.06)	0.0020 (1.30)	0.0065 (3.19)
	Taipei	−0.0049 (−9.53)	−0.0004 (−52.97)	−0.0008 (−29.45)	−0.0037 (−7.69)	0.0009 (1.25)	0.0104 (9.97)	0.0069 (5.64)

The Middle East, India, and North Africa except Cinzana showed an increase of τ_T with time. As shown in Table 2, the rate of annual change of τ_T at Ballia and Kanpur showed a clear tendency to increase. We find 0.0048 $\tau_T yr^{-1}$ and 0.0069 $\tau_T yr^{-1}$, respectively. In most North Africa and the Middle East regions, the change rate of τ_T (-0.006 to 0.0020 $\tau_T yr^{-1}$) is lower than other regions; however, τ_T of Tamanrasset sites increased as 0.0108 $\tau_T yr^{-1}$) because of τ_D. It is supported by the results from El-Metwally et al., 2020 [66]. The authors conclude that Tamanrasset is the site most affected by dust from the downwind Saharan sources in the Saharan/Arabian region.

Other studies also confirmed this trend of regional τ_T change. Balarabe et al. (2016) reported that, based on AERONET data, there were no remarkable AOD trends for the period from 1998 to 2013 over Ilorin, Nigeria [44]. Maghrabi and Alotaibi (2018) reported a significant increase of approximately 0.119 of the annual mean AOD at 500 nm measured by AERONET sunphotometer in the central Arabian Peninsula from 1999 to 2015 [67]. Klingmüller et al. (2016) also stated that AOD increased in Saudi Arabia between 2001 and 2012 [68]. In addition, the change in the concentration of particulate matter, expressed by AOD, was attributed to different aerosol types. The authors identified the following aerosol types in decreasing order of importance: biomass burning, anthropogenic pollution, and soil emission. Meteorological conditions played a significant role, too [14,63,69,70].

The annual mean of dust-only AOD (τ_D) was high in North Africa, naturally, because dust is a major aerosol type in that part of the world. We find low values of τ_D in Southeast Asia, see Figure 2. In the India and Northeast Asia region except for Beijing, the annual change of τ_D tended to decrease from -0.0004 to -0.0022 $\tau_D yr^{-1}$ (Table 2). In case of Beijing, τ_D increased by 22.52% (0.0011 $\tau_D yr^{-1}$). In Europe, Middle East Asia, and North Africa,

the annual rate of change increased from 0.0002 to 0.0133 $\tau_D yr^{-1}$. The exception is Ilorin, where we find −0.27% (−0.0001 $\tau_D yr^{-1}$) because this region is located in the southern part among measurement site in North Africa; thus, the least affected by Saharan dust.

We assume that non-dust AOD values describe anthropogenic emissions and local biomass burning. Anthropogenic emissions mainly belong to the fine-mode fraction of the particle size distribution; therefore, denote their contribution to AOD as τ_{PF}. In contrast, locally emitted particles from biomass burning belong to the coarse-mode fraction of pollution. We denote this part of AOD as τ_{PC}.

The annual average values of τ_{PC} slightly increased in Europe, North Africa, and India, and decreased in the Middle East and Northeast Asia. We find values between −0.0015 and 0.0021 $\tau_{PC} yr^{-1}$. We also considered percent variations to compare the rate of change by region, because the rate of change depends on the initial value. Especially, it is difficult to confirm the evident change of τ_{PC} values in Europe and India since τ_{PC} are low values itself, but the percent variation in Thessaloniki and Ballia was high as 11.94% and 10.53%, respectively.

The annual average value of τ_{PF} also varied by region. The mean changes of τ_{PF} (at 440 nm) for the observation site in India show a clear tendency towards increasing values. We find 0.0055 $\tau_{PF} yr^{-1}$ for Ballia and 0.0019 $\tau_{PF} yr^{-1}$ for Kanpur. In the other regions, except for Erdemli (Europe), Ilorin, Tamanrasset (North Africa), and Sede Boker (Middle East), the changes of mean τ_{PF} tended to decrease significantly compared to τ_D and τ_{PC}. We find values between −0.0011 to −0.0142 $\tau_{PF} yr^{-1}$. The stations at Erdemli, Ilorin, Tamanrasset, and Sede Boker showed a slight increase of τ_{PF}, i.e., 0.0005, 0.0024, 0.0001, and 0.0008 $\tau_{PF} yr^{-1}$, respectively.

In the next step, we analyzed changes of τ (increase and decrease) in terms of aerosol types. We used in our analysis the percent variation of τ_T, τ_D, τ_{PC}, and τ_{PF} (see Equation (7)), respectively. We find a decline of τ_T and τ_{PF} in Europe. We find comparably high confidence levels of 95% (based on MK-test) for the stations in Thessaloniki and Venice, see Table 3. In addition, the slope of τ_D in Thessaloniki and Venice (using the linear-regression method) was 0.0037 $\tau_D yr^{-1}$ and 0.0012 $\tau_D yr^{-1}$, but the percent variation was as high as 112.29% (Thessaloniki) and 125.22% (Venice).

τ_T decreased for the Asian stations, in a similar fashion to the sites in Europe. However, this change of τ_T was different for the Southeast and Northeast Asian stations if we take account of the aerosol types. With respect to Southeast Asia, the decrease of τ_T seems to be mainly caused by a decrease in emissions of fine-mode particles. In Northeast Asia, changes in τ showed different characteristics according to region. The MK-test shows 95% confidence level for the trends observed for τ_T (Beijing and Osaka), τ_D (Osaka), τ_{PC} (Seoul and Osaka), and τ_{PF} (Beijing and Osaka). Non-dust coarse-mode particles are emitted from sources related to anthropogenic activities, e.g., traffic and plants. Regulations on emissions of air pollution thus may be responsible for the lower concentrations of this type of coarse-mode particles [11,63].

In the case of Beijing, which is affected by high levels of air pollution, τ_D increased by 22.52% (0.0011 $\tau_D yr^{-1}$). The non-dust part of AOD, and particularly the AOD related to fine-mode particles (τ_{PF}), seemed to decrease by −21.43% (−0.0142 $\tau_{PF} yr^{-1}$). Thus, taking account of all three components, we find that the decrease of fine-mode pollution mainly causes a decrease in total AOD. This result is similar to results reported in previous research [10]. The authors show that black carbon in China decreased due to the strict policy of reduction of pollution emissions. Li et al. (2015) furthermore stated that dust aerosol concentrations had increased between 2002 and 2006 but then remained constant between 2008 and 2013.

Table 3. MK-test results in terms of number of data points (n), Z-value, *p*-value, and Sen's slope (S) of τ (440 nm) according to aerosol type. The Z-value follows the standard normal distribution and explains the significance of the trend. The *p*-value decides on the significance of the hypothesis (from highly likely to highly unlikely) depending on the significance level. S is Sen's slope estimator and means the degree of increase or decrease in trend.

Region	Site	n	τ_T			τ_D			τ_{PC}			τ_{PF}		
			Z	*p*	S	Z	*p*	S	Z	*p*	S	Z	*p*	S
Europe	Thessaloniki	14	**−2.5183** *	0.0118	−0.005	1.3139	0.1889	0.0034	0.219	0.8267	0.0001	**−2.9562** *	0.0031	−0.008
	Venice	18	**−3.0302** *	0.0024	−0.0084	**2.3484** *	0.0189	0.0013	−0.0758	0.9396	−0.0001	**−3.3332** *	0.0009	−0.0109
	Erdemli	10	0.1789	0.858	0.0009	0.3578	0.7205	0.0006	−0.3578	0.7205	−0.0009	0	1	−0.0003
North Africa	Cape Verde	16	0	1	0	0.045	0.9641	0.0002	**2.1161** *	0.0343	0.0019	−1.2156	0.2241	−0.0012
	Cinzana	15	−0.099	0.9212	−0.0011	−0.099	0.9212	−0.0004	0	1	0.0002	−1.1396	0.2545	−0.0021
	Ilorin	11	−0.3114	0.7555	−0.0011	0	1	−0.0011	−0.4671	0.6404	−0.0035	0	1	0.0029
	Tamanrasset	9	1.5639	0.1179	0.0134	1.3553	0.1753	0.0135	0.7298	0.4655	0.0013	0.5213	0.6022	0.0023
Middle East	Sede Boker	15	0.7918	0.4285	0.0023	0.3959	0.6922	0.0026	0	1	0	0.4949	0.6207	0.0013
	Mezaira	11	1.0899	0.2758	0.0081	0.9342	0.3502	0.0084	−0.3114	0.7555	−0.00031	0	1	0
India	Ballia	10	0.8944	0.3711	0.013	−0.3578	0.7205	−0.0024	0	1	0.00048	1.0733	0.2831	0.0188
	Kanpur	17	**2.7599** *	0.0058	0.0094	−1.0298	0.3031	−0.0026	0	1	0	**2.0184** *	0.0436	0.0103
Southeast Asia	Chiang Mai	9	0.7298	0.4655	0.0074	−0.1789	0.858	−0.0001	0.3578	0.7205	0.00052	0.1789	0.858	0.0026
	Bangkok	9	**1.9809** *	0.0476	0.0099	−0.5367	0.5915	−0.0002	0	1	−0.00001	1.0733	0.2831	0.0065
Northeast Asia	Beijing	16	**−2.1161** *	0.0343	−0.0148	0.4953	0.6204	0.0015	−0.4953	0.6204	−0.00047	**−2.1161** *	0.0343	−0.0144
	Seoul	18	−0.6818	0.4954	−0.0042	−1.3636	0.1727	−0.0012	**−2.9545** *	0.0031	−0.00117	−0.606	0.5445	−0.0029
	Osaka	9	**−3.0235** *	0.0025	−0.0209	**−2.3062** *	0.0211	−0.0019	**−2.3062** *	0.0211	−0.00193	**−3.2320** *	0.0012	−0.0206
	Taipei	13	−1.4032	0.1606	−0.0091	−0.79312	0.4277	−0.0004	−1.2812	0.2001	−0.00114	−1.1592	0.2464	−0.0076

* denotes clear trend with 95% confidence level, $|z| > 1.96$.

The annual change of τ_T for the stations in North Africa increased during (0.0006–0.0108 $\tau_T yr^{-1}$) over ten more years. The exception is the station at Cinzana. The properties of the variations seem to be different for the different regions. The percent variation of the τ_T increase at Tamanrasset is quite obviously related to a change of τ_D. The Cape Verde and Ilorin stations showed a slightly increasing trend, most likely caused by a change of coarse- and fine-mode particles. Cinzana is the only site of all North African stations where we find a decrease of τ_T. This decrease seems to be driven by a decrease in τ_{PF}.

The τ_D in the Middle East increased, which resulted in an increase of total optical depth. In the case of India, the change of τ_T is related to a decrease in τ_D and an increase in τ_{PC} and τ_{PF}. The increase in τ_{PC} and τ_{PF} may be associated with new policies related to aerosol emissions in the Indian regions considered in this study [70,71].

A comprehensive graph of the annual average, the overall increase, and the percent variation associated with total, dust-only, and coarse- and fine-mode pollution AOD is presented in Figure 3.

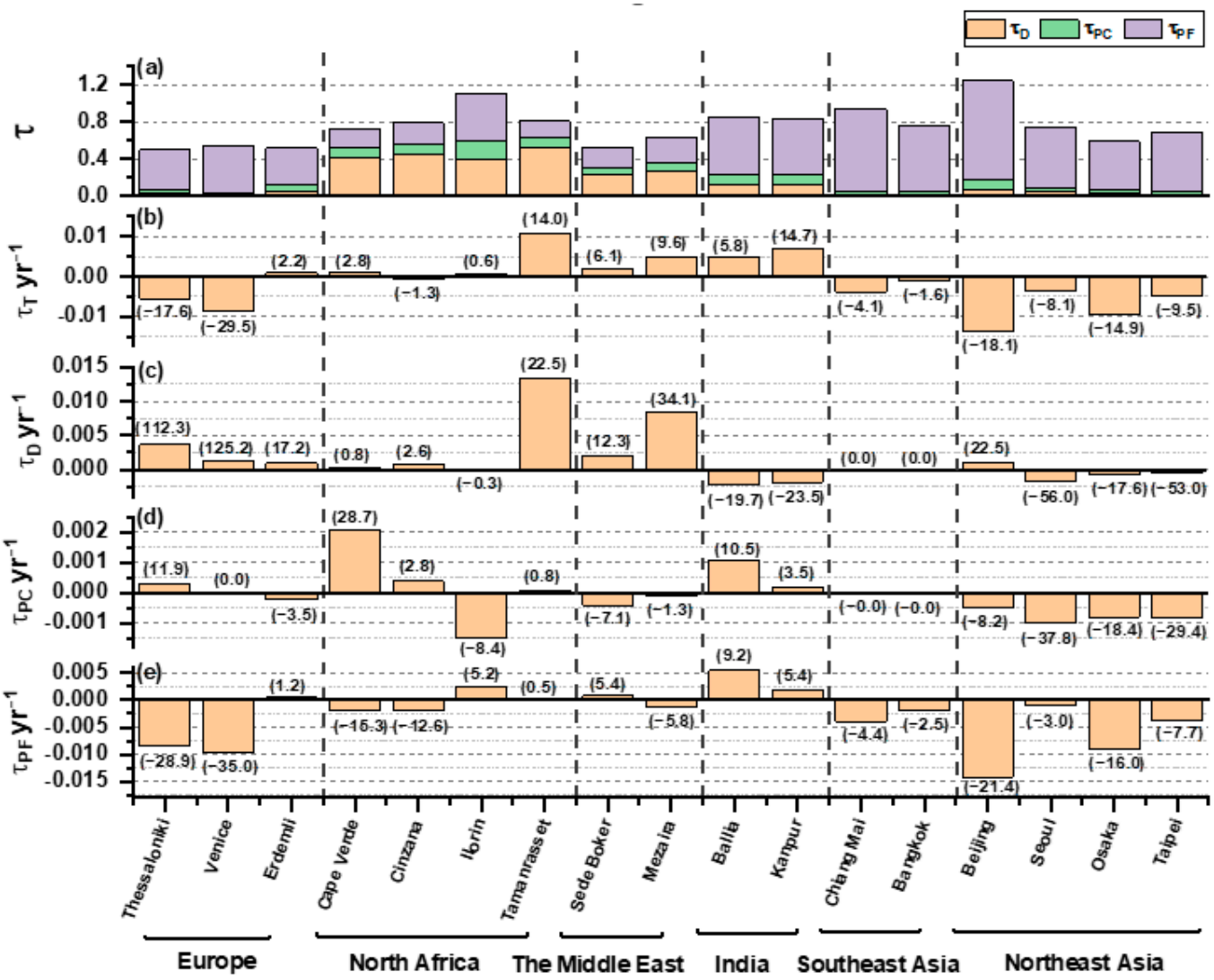

Figure 3. (**a**) Average AOD in terms of dust and coarse- and fine-mode pollution AOD, and the change of annual values of (**b**) total AOD (τ_T), (**c**) dust-only AOD (τ_D), (**d**) coarse-mode pollution AOD (τ_{PC}), and (**e**) fine-mode pollution AOD (τ_{PF}). The values inside the brackets present the percent variation for each of the 17 sites.

3.3. Ångström Exponent and FMF: Annual Trends

Our analysis shows regional differences in aerosol type and size changes which can be inferred from annual mean values of AOD, see Table 2. In addition to this result, we examined the change of particle size distribution, especially that of fine-mode particles, more closely by using the Ångström exponent of total (α_T) and fine-mode particles (α_{PF}) and the FMF (fine-mode fraction). The changes of α_T and α_{PF} also can be seen in Supplementary Figures S6 and S7. The value of α_{PF} indicates the presence of anthropogenic pollution particles. FMF describes the fraction of fine-mode particles compared to all particles in the atmospheric column observed by the sun photometer (Table 2). Figure 4 shows the comprehensive results of the average value, the increasing rate, and the percent variation of α_T and α_{PF}.

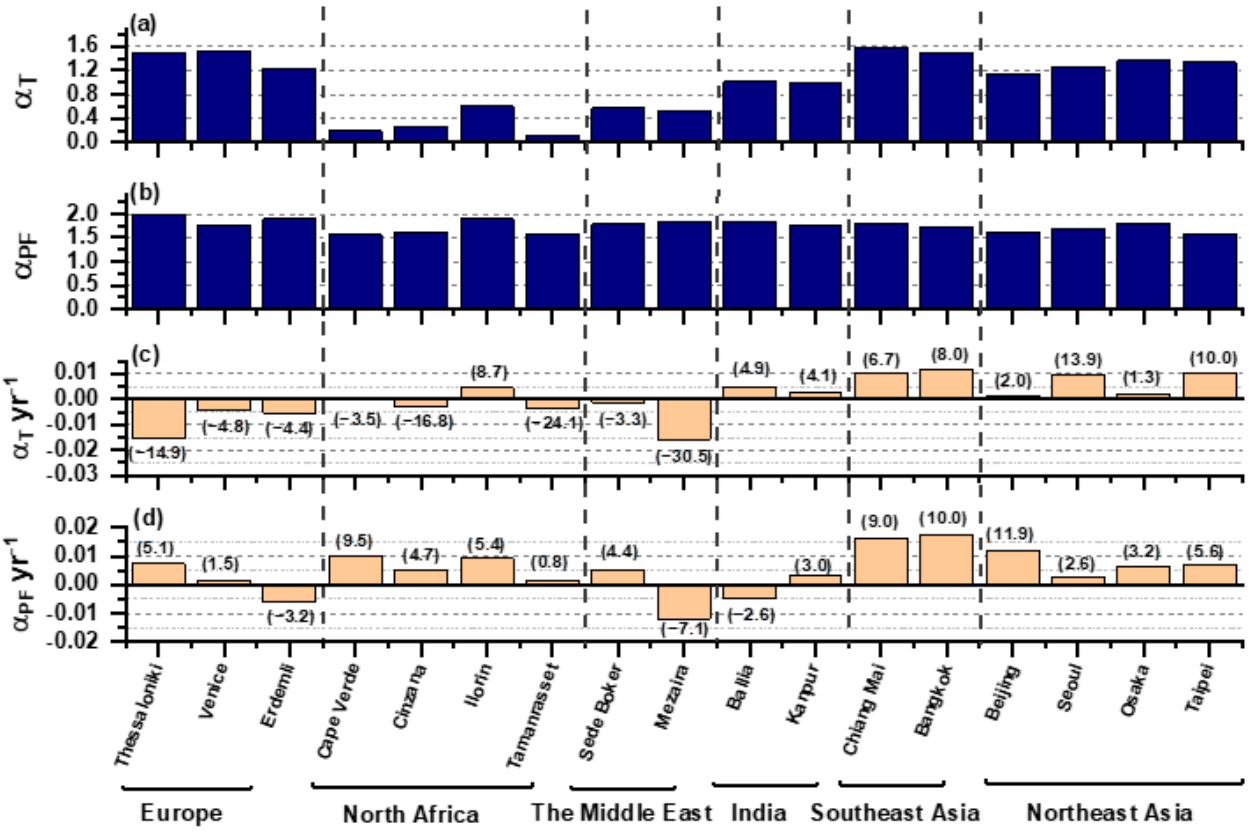

Figure 4. Average Ångström exponent (α) of (**a**) total and (**b**) fine-mode pollution particles, and the change of the annual values of the (**c**) total Ångström exponent (α_T) and (**d**) fine-mode pollution Ångström exponent (α_{PF}). The values inside the brackets present the percent variation for each of the 17 sites.

The α_T in Europe, North Africa, and the Middle East regions except Ilorin decreased during the research period we analyzed. We find negative values ranging from −3.30% to −30.47%. FMF decreased by −3.74% to −21.15%. These trends show that the particles on average became larger. This result is similar to the main findings discussed in the previous section, where we showed that τ_D and τ_{PC} increased and τ_{PF} decreased. These changes are associated with increased levels of dust particle concentration and reduced levels of fine-mode particles due to climate change [63,68,72] and environmental regulations [10,11,13,14]. The Ilorin site in Nigeria is different from the other North African regions. Ilorin is located in the transition zone between the humid tropical area (South Africa) and the semi-arid area (North Africa) [73,74]. This site also exhibits an increase in anthropogenic emissions caused by the rapid increase of population and economic growth [44].

Additionally, we checked if changes of α_{PF} corroborate our assumption that characteristics of the size distribution of the fine-mode particles also changed. The values of α_{PF} in Europe, North Africa, and the Middle East except Erdemli (Turkey) and Mezaira (UAE) show positive trends, i.e., 0.0015 yr^{-1} to 0.0101 yr^{-1}. These increases indicate that the size of the fine-mode particles became smaller.

The annual mean of α_T at Ballia and Kanpur increased in 0.0050 yr^{-1} (4.93%) and 0.0024 yr^{-1} (4.08%), respectively. These increases indicate that particle size became smaller. The increase of the FMF value corroborates this result. The values of α_{PF} showed a positive trend at the Kanpur site, which means that fine-mode particles became smaller over the course of several years. The negative values of α_{PF} in Ballia might be caused by the comparably few data points available for the first few years of observations (Supplementary Table S1). Kanpur is a highly polluted city in the Indo-Gangetic region [75,76] which may explain in large part the high concentration of small particles in this region.

In Southeast Asia, the values of α_T increased. We find 0.0105 yr^{-1} (6.68%) at Chiang Mai and 0.0119 yr^{-1} (8.03%) in Bangkok. The α_{PF} showed a more increasing trend compared to α_T as 0.0163 yr^{-1} (8.99%) and 0.0175 yr^{-1} (10.03%) at Chiang Mai and Bangkok, respectively, and also had clear trend in MK-test (Table 4). On the contrary, FMF showed a negative trend as -0.0022 yr^{-1} (-0.91%) at Ching Mai and -0.0002 yr^{-1} (-0.08%) at Bangkok. Considering that the major aerosols in Southeast Asia are biomass burning aerosol and anthropogenic aerosol composed of fine-mode aerosol, it is estimated that the particle size of these two types is continuously decreasing [14,63,70,71].

The values of α_T in Northeast Asia differ to 1.30–13.94% depending on stations. For example, Seoul and Taipei had highly positive increases in α_T. That positive increases could be related to reducing the dust concentration, which would lead to a significant decrease of τ_{PC} compared to that of τ_{PF}. For Beijing, the α_T slightly increased compared to the other sites because of τ_D increase and a slight decrease of τ_{PC}. Thus, we come to the conclusion that the increase of α_T most likely was caused by a change in the atmosphere's dust load.

The α_{PF} values in the Asian region increased by 2.57% to 11.92% (0.0024 to 0.0122 yr^{-1}) over the observation periods considered in our study. The data indicate that fine-mode particle size became smaller over the years and that this change might also be related to changes in the chemical composition of the pollution particles. Joo et al., 2021 reported that extinction efficiencies in Korea increased although the $PM_{2.5}$ mass concentration decreased. This result suggests that even though the $PM_{2.5}$ concentration decreased compared to the past, either particle size of $PM_{2.5}$ became smaller or the number of particles with high scattering efficiency increased [77]. Uno et al., 2020 stated that the chemical composition of aerosols in East Asia changed significantly [78]. With regard to regions downwind of China, sulfate (accumulation mode) concentrations decreased significantly, and nitrate (accumulation–coarse mode) concentrations increased [79]. These results show that there clearly is a need to conduct more long-term studies on the relationship between aerosol mass and optical density, size distribution, and chemical composition.

Table 4. MK-test results in terms of number of data points (m), Z value, *p*-value, and Sen's slope (S) of FMF, α_T and α_{PF}. Meaning of parameters same as in Table 4.

Region	Site	n	FMF			α_T			α_{PF}		
			Z	***p***	**S**	**Z**	***p***	**S**	**Z**	***p***	**S**
Europe	Thessaloniki	14	**−2.1898** *	0.0285	−0.0108	−1.4234	0.1546	−0.0168	1.0949	0.2736	0.0075
	Venice	18	**−2.1969** *	0.028	−0.0031	−0.9848	0.3247	−0.0058	−0.303	0.7619	−0.002
	Erdemli	10	−0.3578	0.7205	−0.0019	−0.3578	0.7205	−0.0087	−0.5367	0.5915	−0.0083
North Africa	Cape Verde	16	**−1.8459** **	0.0649	−0.0028	−0.1351	0.8926	−0.0008	**2.5733** *	0.0101	0.0141
	Cinzana	15	−0.5939	0.5526	−0.0013	−1.1877	0.235	−0.0031	1.4846	0.1376	0.0073
	Ilorin	11	0.1557	0.8763	0.0027	0.1557	0.8763	0.0053	**1.8684** **	0.0617	0.0115
	Tamanrasset	9	−0.7298	0.4655	−0.0033	−0.9383	0.3481	−0.005	0	1	−0.0006
Middle East	Sede Boker	15	−0.099	0.9212	−0.002	0.099	0.9212	0.0006	1.2867	0.6207	0.0075
	Mezaira	11	−0.4671	0.6404	−0.0097	−0.7785	0.4363	−0.0121	−1.557	0.1195	−0.0203
India	Ballia	10	0.1789	0.858	0.005	0.1789	0.858	0.0068	−0.5367	0.5915	−0.0026
	Kanpur	17	1.3594	0.174	0.0048	0.6179	0.5366	0.0048	−0.206	0.8368	−0.0008
Southeast Asia	Chiang Mai	10	0.0000	1.0000	0.0006	0.6179	0.5366	0.0128	**1.9677** *	0.0491	0.0157
	Bangkok	10	0.3578	0.7205	0.0005	1.61	0.1074	0.012	**2.3255** *	0.02	0.0199
Northeast Asia	Beijing	16	−0.5939	0.5526	−0.0026	0.7654	0.444	0.0019	**2.9265** *	0.0034	0.0119
	Seoul	18	**1.6666** **	0.0956	0.0021	**2.2727** *	0.0231	0.0095	0.9848	0.3247	0.0022
	Osaka	9	−0.7298	0.4655	−0.0011	0.1043	0.917	0.0006	1.1468	0.2515	0.0109
	Taipei	13	0.7931	0.4277	0.0016	**3.5995** *	0.0003	0.0113	1.4032	0.1606	0.0089

* denotes that clear trend with 95% confidence level, $|z| > 1.96$ and ** means clear trend with 90% confidence level, $|z| > 1.65$.

4. Summary and Conclusions

We analyzed trends in regional AOD based on separating aerosols into dust and coarse- and fine-mode pollution particles for 17 AERONET observation sites. Mainly, we focused on the change in AOD and Ångström exponents of fine-mode pollution particles (τ_{PF} and α_{PF}). The following key results were obtained:

- The change characteristics of τ_D, τ_{PC}, and τ_{PF} are different for each region. In Europe and Asia, the decrease in τ_T was remarkable due to effects caused by new air quality policies. The τ_D increased near the Sahara region.
- The τ_{PF} mainly decreased in Europe and Southeast Asia, whereas τ_{PC} decreased in the Middle East and Northeast Asia. τ_{PC} and τ_{PF} are related to non-dust AOD. Thus, we assume that changes related to the practical policymaking have on air pollution emissions.
- The mean size of particle size distribution became larger in Europe, the Middle East, and North Africa because of emissions of dust particles. On the other hand, the mean particle size became smaller in India and Southeast Asia. We assume that this reduction of particle size is primarily related to the change in the concentration of fine-mode particles.
- The changes of α_{PF} show that the size of fine-mode particles emitted from anthropogenic pollution most likely became smaller compared to particle size in past times in the regions we investigated here. We believed that the size change of fine-mode particles might be related to secondary aerosols, and it can cause adverse effects on visibility and human health.

Particle size and characteristics are essential to understanding air pollution and visibility and have changed over the past decade or more, but few studies about those properties. The information on the characteristics of aerosols helps to find emission sources and how to remove them effectively. Therefore, we need more studies paying attention to changes in the size and quantity of fine-mode pollution particles to reflect air pollution policy.

Supplementary Materials: The following supporting information can be downloaded at: https://www.mdpi.com/article/10.3390/rs14184429/s1, Figure S1. Correlation coefficient, R^2 between dust ratio (R_D) at wavelength 1020 nm and coarse mode fraction of the particle size distributions for each of the AERONET sites; Figure S2. Annual trend of total AOD (τ_T) at wavelength 440 nm for the 17 AERONET sites for the timeframe from 2001–2018; Figure S3. Annual trend of dust-only AOD (τ_D) at wavelength 440 nm for the 17 AERONET sites for the timeframe from 2001–2018; Figure S4. Annual trend of coarse-mode pollution AOD (τ_{PC}) at wavelength 440 nm for the 17 AERONET sites for the timeframe from 2001–2018; Figure S5. Annual trend of fine-mode pollution AOD (τ_{PF}) at wavelength 440 nm for the 17 AERONET sites for the timeframe from 2001–2018; Figure S6. Annual trend of the total Ångström exponent (α_T) for the wavelength interval 440–870 nm for the 17 AERONET sites for the timeframe from 2001–2018; Figure S7. Annual trend of the Ångström exponent of fine-mode pollution particles (α_{PF}) for the wavelength interval 440–870 nm for the 17 AERONET sites for the timeframe from 2001–2018; Table S1. Number of observation days in each year for the 17 AERONET Sun/sky radiometer sites (version 3 level 2.0 data).

Author Contributions: Conceptualization Y.N.; methodology and software, S.-K.S. and D.S.; formal analysis and investigation, J.S. (Juseon Shin) and J.S. (Juhyeon Sim); collected resources, N.D., S.J., T.K. and G.K.; writing—original draft preparation, J.S. (Juseon Shin); writing—review and editing, D.M. and M.T.; supervision and project administration, Y.N.; funding acquisition, Y.N. All authors have read and agreed to the published version of the manuscript.

Funding: This work was supported by the "Graduate School of Particulate Matter Specialization" of Korea Environmental Industry & Technology Institute grant funded by the Ministry of Environment, Republic of Korea, and by the National Research Foundation of Korea (NRF) grant funded by the Korean government (MSIT, MOE) and (Grant No. 2019M3E7A1113103).

Institutional Review Board Statement: Not applicable.

Informed Consent Statement: Not applicable.

Data Availability Statement: The data presented in this study are available on request from the corresponding author.

Acknowledgments: We thank the PIs of the AERONET group for providing their data to the community. We would also like to thank AERONET for their efforts in offering high-quality data and derivative products. All data used in this are in the AERONET homepage at https://aeronet.gsfc.nasa.gov/ (accessed on 9 January 2020).

Conflicts of Interest: The authors declare no conflict of interest.

References

1. Ramanathan, V.; Ramana, M.V.; Roberts, G.; Kim, D.; Corrigan, C.; Chung, C.; Winker, D. Warming trends in Asia amplified by brown cloud solar absorption. *Nature* **2007**, *448*, 575–578. [CrossRef] [PubMed]
2. Ramanathan, V.; Carmichael, G. Global and regional climate changes due to black carbon. *Nat. Geosci.* **2008**, *1*, 221–227. [CrossRef]
3. Arneth, A. *Climate Change and Land: An IPCC Special Report on Climate Change, Desertification, Land Degradation, Sustainable Land Management, Food Security, and Greenhouse Gas Fluxes in Terrestrial Ecosystems*; IPCC: Geneva, Switzerland, 2019.
4. World Health Organization. *WHO Expert Consultation: Available Evidence for the Future Update of the WHO Global Air Quality Guidelines (AQGs): Meeting Report Bonn, Germany 29 September–1 October 2015*; No. WHO/EURO: 2016-2665-42421-58848; World Health Organization, Regional Office for Europe: Geneva, Switzerland, 2016.
5. Schraufnagel, D.E.; Balmes, J.R.; Cowl, C.T.; De Matteis, S.; Jung, S.H.; Mortimer, K.; Perez-Padilla, R.; Rice, M.B.; Riojas-Rodriguez, H.; Sood, A.; et al. Air Pollution and Noncommunicable Diseases: A Review by the Forum of International Respiratory Societies' Environmental Committee, Part 1: The Damaging Effects of Air Pollution. *Chest* **2019**, *155*, 409–416. [CrossRef] [PubMed]
6. Loomis, D.; Grosse, Y.; Lauby-Secretan, B.; Ghissassi, F.E.; Bouvard, V.; Benbrahim-Tallaa, L.; Guha, N.; Baan, R.; Mattock, H.; Straif, K. The carcinogenicity of outdoor air pollution. *Lancet Oncol.* **2013**, *14*, 1262–1263. [CrossRef]
7. WHO. *WHO Global Air Quality Guidelines: Particulate Matter (PM2.5 and PM10), Ozone, Nitrogen Dioxide, Sulfur Dioxide and Carbon Monoxide: Executive Summary*; WHO: Geneva, Switzerland, 2021.
8. Collaud Coen, M.; Andrews, E.; Asmi, A.; Baltensperger, U.; Bukowiecki, N.; Day, D.; Fiebig, M.; Fjaeraa, A.M.; Flentje, H.; Hyvärinen, A.; et al. Aerosol decadal trends—Part 1: In-situ optical measurements at GAW and IMPROVE stations. *Atmos. Chem. Phys.* **2013**, *13*, 869–894. [CrossRef]
9. Li, J.; Carlson, B.E.; Dubovik, O.; Lacis, A.A. Recent trends in aerosol optical properties derived from AERONET measurements. *Atmos. Chem. Phys.* **2014**, *14*, 12271–12289. [CrossRef]
10. Li, Z.; Li, L.; Zhang, F.; Li, D.; Xie, Y.; Xu, H. Comparison of aerosol properties over Beijing and Kanpur: Optical, physical properties and aerosol component composition retrieved from 12 years ground-based Sun-sky radiometer remote sensing data. *J. Geophys. Res. Atmos.* **2015**, *120*, 1520–1535. [CrossRef]
11. Mehta, M.; Singh, N.; Anshumali. Global trends of columnar and vertically distributed properties of aerosols with emphasis on dust, polluted dust and smoke—Inferences from 10-year long CALIOP observations. *Remote Sens. Environ.* **2018**, *208*, 120–132. [CrossRef]
12. Yang, X.; Jiang, L.; Zhao, W.; Xiong, Q.; Zhao, W.; Yan, X. Comparison of Ground-Based PM2.5 and PM10 Concentrations in China, India, and the U.S. *Int. J. Environ. Res. Public Health* **2018**, *15*, 1382. [CrossRef]
13. Pozzer, A.; Bacer, S.; Sappadina, S.D.Z.; Predicatori, F.; Caleffi, A. Long-term concentrations of fine particulate matter and impact on human health in Verona, Italy. *Atmos. Pollut. Res.* **2019**, *10*, 731–738. [CrossRef]
14. Chirasophon, S.; Pochanart, P. The Long-term Characteristics of PM10 and PM2.5 in Bangkok, Thailand. *Asian J. Atmos. Environ.* **2020**, *14*, 73–83. [CrossRef]
15. Liu, J.; Ren, C.; Huang, X.; Nie, W.; Wang, J.; Sun, P.; Chi, X.; Ding, A. Increased Aerosol Extinction Efficiency Hinders Visibility Improvement in Eastern China. *Geophys. Res. Lett.* **2020**, *47*, e2020GL090167. [CrossRef]
16. Lee, K.-H.; Muller, D.; Noh, Y.-M.; Shin, S.-K.; Shin, D.-H. Depolarization ratio retrievals using AERONET sun photometer data. *J. Opt. Soc. Korea* **2010**, *14*, 178–184. [CrossRef]
17. Burton, S.; Vaughan, M.; Ferrare, R.; Hostetler, C. Separating mixtures of aerosol types in airborne High Spectral Resolution Lidar data. *Atmos. Meas. Tech.* **2014**, *7*, 419–436. [CrossRef]
18. Han, T.; Xu, W.; Chen, C.; Liu, X.; Wang, Q.; Li, J.; Zhao, X.; Du, W.; Wang, Z.; Sun, Y. Chemical apportionment of aerosol optical properties during the Asia-Pacific Economic Cooperation summit in Beijing, China. *J. Geophys. Res. Atmos.* **2015**, *120*, 12–281. [CrossRef]
19. Hatakeyama, S. Aerosols. In *Air Pollution Impacts on Plants in East Asia*; Izuta, T., Ed.; Springer: Tokyo, Japan, 2017; pp. 21–42. [CrossRef]
20. Kitamori, Y.; Mochida, M.; Kawamura, K. Assessment of the aerosol water content in urban atmospheric particles by the hygroscopic growth measurements in Sapporo, Japan. *Atmos. Environ.* **2009**, *43*, 3416–3423. [CrossRef]
21. Cheng, Y.-H.; Li, Y.-S. Influences of Traffic Emissions and Meteorological Conditions on Ambient PM10 and PM2.5 Levels at a Highway Toll Station. *Aerosol Air Qual. Res.* **2010**, *10*, 456–462. [CrossRef]

22. Xue, J.; Griffith, S.M.; Yu, X.; Lau, A.K.H.; Yu, J.Z. Effect of nitrate and sulfate relative abundance in PM2.5 on liquid water content explored through half-hourly observations of inorganic soluble aerosols at a polluted receptor site. *Atmos. Environ.* **2014**, *99*, 24–31. [CrossRef]
23. Mesquita, S.R.; Dachs, J.; van Drooge, B.L.; Castro-Jimenez, J.; Navarro-Martin, L.; Barata, C.; Vieira, N.; Guimaraes, L.; Pina, B. Toxicity assessment of atmospheric particulate matter in the Mediterranean and Black Seas open waters. *Sci. Total Environ.* **2016**, *545*, 163–170. [CrossRef]
24. Tan, H.; Cai, M.; Fan, Q.; Liu, L.; Li, F.; Chan, P.W.; Deng, X.; Wu, D. An analysis of aerosol liquid water content and related impact factors in Pearl River Delta. *Sci. Total Environ.* **2017**, *579*, 1822–1830. [CrossRef]
25. Xu, L.; Duan, F.; He, K.; Ma, Y.; Zhu, L.; Zheng, Y.; Huang, T.; Kimoto, T.; Ma, T.; Li, H.; et al. Characteristics of the secondary water-soluble ions in a typical autumn haze in Beijing. *Environ. Pollut.* **2017**, *227*, 296–305. [CrossRef] [PubMed]
26. Kong, L.; Du, C.; Zhanzakova, A.; Cheng, T.; Yang, X.; Wang, L.; Fu, H.; Chen, J.; Zhang, S. Trends in heterogeneous aqueous reaction in continuous haze episodes in suburban Shanghai: An in-depth case study. *Sci. Total Environ.* **2018**, *634*, 1192–1204. [CrossRef] [PubMed]
27. Kudo, S.; Iijima, A.; Kumagai, K.; Tago, H.; Ichijo, M. An exhaustive classification for the seasonal variation of organic peaks in the atmospheric fine particles obtained by a gas chromatography/mass spectrometry. *Environ. Technol. Innov.* **2018**, *12*, 14–26. [CrossRef]
28. Wang, H.; Ding, J.; Xu, J.; Wen, J.; Han, J.; Wang, K.; Shi, G.; Feng, Y.; Ivey, C.E.; Wang, Y.; et al. Aerosols in an arid environment: The role of aerosol water content, particulate acidity, precursors, and relative humidity on secondary inorganic aerosols. *Sci. Total Environ.* **2019**, *646*, 564–572. [CrossRef] [PubMed]
29. Cherian, R.; Quaas, J. Trends in AOD, Clouds, and Cloud Radiative Effects in Satellite Data and CMIP5 and CMIP6 Model Simulations Over Aerosol Source Regions. *Geophys. Res. Lett.* **2020**, *47*, e2020GL087132. [CrossRef]
30. Dehkhoda, N.; Noh, Y.; Joo, S. Long-Term Variation of Black Carbon Absorption Aerosol Optical Depth from AERONET Data over East Asia. *Remote Sens.* **2020**, *12*, 3551. [CrossRef]
31. Dubovik, O.; Holben, B.; Lapyonok, T.; Sinyuk, A.; Mishchenko, M.; Yang, P.; Slutsker, I. Non-spherical aerosol retrieval method employing light scattering by spheroids. *Geophys. Res. Lett.* **2002**, *29*, 54-1–54-4. [CrossRef]
32. Omar, A.H.; Won, J.G.; Winker, D.M.; Yoon, S.C.; Dubovik, O.; McCormick, M.P. Development of global aerosol models using cluster analysis of Aerosol Robotic Network (AERONET) measurements. *J. Geophys. Res. Atmos.* **2005**, *110*, D10S14. [CrossRef]
33. Levy, R.C.; Remer, L.A.; Dubovik, O. Global aerosol optical properties and application to Moderate Resolution Imaging Spectroradiometer aerosol retrieval over land. *J. Geophys. Res. Atmos.* **2007**, *112*, D13. [CrossRef]
34. Mielonen, T.; Arola, A.; Komppula, M.; Kukkonen, J.; Koskinen, J.; De Leeuw, G.; Lehtinen, K. Comparison of CALIOP level 2 aerosol subtypes to aerosol types derived from AERONET inversion data. *Geophys. Res. Lett.* **2009**, *36*, 18. [CrossRef]
35. Russell, P.; Bergstrom, R.; Shinozuka, Y.; Clarke, A.; DeCarlo, P.; Jimenez, J.; Livingston, J.; Redemann, J.; Dubovik, O.; Strawa, A. Absorption Angstrom Exponent in AERONET and related data as an indicator of aerosol composition. *Atmos. Chem. Phys.* **2010**, *10*, 1155–1169. [CrossRef]
36. Noh, Y.M.; Müller, D.; Mattis, I.; Lee, H.; Kim, Y.J. Vertically resolved light-absorption characteristics and the influence of relative humidity on particle properties: Multiwavelength Raman lidar observations of East Asian aerosol types over Korea. *J. Geophys. Res. Atmos.* **2011**, *116*, D6. [CrossRef]
37. Boselli, A.; Caggiano, R.; Cornacchia, C.; Madonna, F.; Mona, L.; Macchiato, M.; Pappalardo, G.; Trippetta, S. Multi year sun-photometer measurements for aerosol characterization in a Central Mediterranean site. *Atmos. Res.* **2012**, *104*, 98–110. [CrossRef]
38. Rossini, P.; De Lazzari, A.; Guerzoni, S.; Molinaroli, E.; Rampazzo, G.; Zancanaro, A. Atmospheric input of organic pollutants to the Venice Lagoon. *Ann. Chim.* **2001**, *91*, 491–501.
39. Rampazzo, G.; Masiol, M.; Visin, F.; Rampado, E.; Pavoni, B. Geochemical characterization of PM10 emitted by glass factories in Murano, Venice (Italy). *Chemosphere* **2008**, *71*, 2068–2075. [CrossRef] [PubMed]
40. Masiol, M.; Rampazzo, G.; Ceccato, D.; Squizzato, S.; Pavoni, B. Characterization of PM10 sources in a coastal area near Venice (Italy): An application of factor-cluster analysis. *Chemosphere* **2010**, *80*, 771–778. [CrossRef]
41. Gregoris, E.; Barbaro, E.; Morabito, E.; Toscano, G.; Donateo, A.; Cesari, D.; Contini, D.; Gambaro, A. Impact of maritime traffic on polycyclic aromatic hydrocarbons, metals and particulate matter in Venice air. *Environ. Sci. Pollut. Res.* **2016**, *23*, 6951–6959. [CrossRef]
42. Martin, C. Environment: Venice's fragile lagoon. *Nature* **2010**, *467*, 529. [CrossRef]
43. Vouitsis, I.; Amanatidis, S.; Ntziachristos, L.; Kelessis, A.; Petrakakis, M.; Stamos, I.; Mitsakis, E.; Samaras, Z. Daily and seasonal variation of traffic related aerosol pollution in Thessaloniki, Greece, during the financial crisis. *Atmos. Environ.* **2015**, *122*, 577–587. [CrossRef]
44. Balarabe, M.; Abdullah, K.; Nawawi, M. Seasonal Variations of Aerosol Optical Properties and Identification of Different Aerosol Types Based on AERONET Data over Sub-Sahara West-Africa. *Atmos. Clim. Sci.* **2016**, *6*, 13–28. [CrossRef]
45. Ram, K.; Sarin, M.; Tripathi, S. A 1 year record of carbonaceous aerosols from an urban site in the Indo-Gangetic Plain: Characterization, sources, and temporal variability. *J. Geophys. Res. Atmos.* **2010**, *115*, D4. [CrossRef]

46. Shimizu, A.; Sugimoto, N.; Matsui, I.; Arao, K.; Uno, I.; Murayama, T.; Kagawa, N.; Aoki, K.; Uchiyama, A.; Yamazaki, A. Continuous observations of Asian dust and other aerosols by polarization lidars in China and Japan during ACE-Asia. *J. Geophys. Res. Atmos.* **2004**, *109*, D19. [CrossRef]
47. Kashima, S.; Yorifuji, T.; Bae, S.; Honda, Y.; Lim, Y.-H.; Hong, Y.-C. Asian dust effect on cause-specific mortality in five cities across South Korea and Japan. *Atmos. Environ.* **2016**, *128*, 20–27. [CrossRef]
48. Park, J.; Kim, H.; Kim, Y.; Heo, J.; Kim, S.-W.; Jeon, K.; Yi, S.-M.; Hopke, P.K. Source apportionment of PM2.5 in Seoul, South Korea and Beijing, China using dispersion normalized PMF. *Sci. Total Environ.* **2022**, *833*, 155056. [CrossRef] [PubMed]
49. Chen, Y.-S.; Sheen, P.-C.; Chen, E.-R.; Liu, Y.-K.; Wu, T.-N.; Yang, C.-Y. Effects of Asian dust storm events on daily mortality in Taipei, Taiwan. *Environ. Res.* **2004**, *95*, 151–155. [CrossRef] [PubMed]
50. Dubovik, O.; Sinyuk, A.; Lapyonok, T.; Holben, B.N.; Mishchenko, M.; Yang, P.; Eck, T.F.; Volten, H.; Munoz, O.; Veihelmann, B. Application of spheroid models to account for aerosol particle nonsphericity in remote sensing of desert dust. *J. Geophys. Res. Atmos.* **2006**, *111*, D11208. [CrossRef]
51. Noh, Y.; Müller, D.; Lee, K.; Kim, K.; Lee, K.; Shimizu, A.; Sano, I.; Park, C.B. Depolarization ratios retrieved by AERONET sun–sky radiometer data and comparison to depolarization ratios measured with lidar. *Atmos. Chem. Phys.* **2017**, *17*, 6271–6290. [CrossRef]
52. Tesche, M.; Ansmann, A.; Müller, D.; Althausen, D.; Engelmann, R.; Freudenthaler, V.; Groß, S. Vertically resolved separation of dust and smoke over Cape Verde using multiwavelength Raman and polarization lidars during Saharan Mineral Dust Experiment 2008. *J. Geophys. Res. Atmos.* **2009**, *114*, D13. [CrossRef]
53. Noh, Y.M. Single-scattering albedo profiling of mixed Asian dust plumes with multiwavelength Raman lidar. *Atmos. Environ.* **2014**, *95*, 305–317. [CrossRef]
54. Freudenthaler, V.; Esselborn, M.; Wiegner, M.; Heese, B.; Tesche, M.; Ansmann, A.; Müller, D.; Althausen, D.; Wirth, M.; Fix, A. Depolarization ratio profiling at several wavelengths in pure Saharan dust during SAMUM 2006. *Tellus B Chem. Phys. Meteorol.* **2009**, *61*, 165–179. [CrossRef]
55. Shin, S.-K.; Tesche, M.; Kim, K.; Kezoudi, M.; Tatarov, B.; Müller, D.; Noh, Y. On the spectral depolarisation and lidar ratio of mineral dust provided in the AERONET version 3 inversion product. *Atmos. Chem. Phys.* **2018**, *18*, 12735–12746. [CrossRef]
56. Shin, S.-K.; Tesche, M.; Noh, Y.; Müller, D. Aerosol-type classification based on AERONET version 3 inversion products. *Atmos. Meas. Tech.* **2019**, *12*, 3789–3803. [CrossRef]
57. Mann, H.B. Nonparametric tests against trend. *Econom. J. Econom. Soc.* **1945**, *13*, 245–259. [CrossRef]
58. Kendall, M. *Rank Correlation Methods*; Charles Griffin: London, UK, 1975.
59. Salmi, T.; Määttä, A.; Anttila, P.; Ruoho-Airola, T.; Amnell, T. *Detecting Trends of Annual Values of Atmospheric Pollutants by the Mann-Kendall Test and Sen's Slope Estimates MAKESENS—The Excel Template Application*; Report Code FMI-AQ-31; Finnish Meteorological Institute: Helsinki, Finland, 2002.
60. Srivastava, A.; Saran, S. Comprehensive study on AOD trends over the Indian subcontinent: A statistical approach. *Int. J. Remote Sens.* **2017**, *38*, 5127–5149. [CrossRef]
61. Logothetis, S.-A.; Salamalikis, V.; Kazantzidis, A. Aerosol classification in Europe, Middle East, North Africa and Arabian Peninsula based on AERONET Version 3. *Atmos. Res.* **2020**, *239*, 104893. [CrossRef]
62. Janjai, S.; Nunez, M.; Masiri, I.; Wattan, R.; Buntoung, S.; Jantarach, T.; Promsen, W. Aerosol optical properties at four sites in Thailand. *Atmos. Clim. Sci.* **2012**, *2*, 441. [CrossRef]
63. Bridhikitti, A.; Overcamp, T.J. Optical characteristics of southeast Asia's regional aerosols and their sources. *J. Air Waste Manag. Assoc.* **2011**, *61*, 747–754. [CrossRef]
64. Shin, S.-K.; Müller, D.; Lee, C.; Lee, K.; Shin, D.; Kim, Y.; Noh, Y. Vertical variation of optical properties of mixed Asian dust/pollution plumes according to pathway of air mass transport over East Asia. *Atmos. Chem. Phys.* **2015**, *15*, 6707–6720. [CrossRef]
65. Liu, D.; Zhao, T.; Boiyo, R.; Chen, S.; Lu, Z.; Wu, Y.; Zhao, Y. Vertical Structures of Dust Aerosols over East Asia Based on CALIPSO Retrievals. *Remote Sens.* **2019**, *11*, 701. [CrossRef]
66. El-Metwally, M.; Korany, M.; Boraiy, M.; Ebada, E.; Wahab, M.A.; Hungershoefer, K.; Alfaro, S. Evidence of anthropization of aerosols in the Saharan and peri-Saharan regions: Implications for the atmospheric transfer of solar radiation. *J. Atmos. Sol. Terr. Phys.* **2020**, *199*, 105199. [CrossRef]
67. Maghrabi, A.; Alotaibi, R. Long-term variations of AOD from an AERONET station in the central Arabian Peninsula. *Theor. Appl. Climatol.* **2018**, *134*, 1015–1026. [CrossRef]
68. Klingmüller, K.; Pozzer, A.; Metzger, S.; Stenchikov, G.L.; Lelieveld, J. Aerosol optical depth trend over the Middle East. *Atmos. Chem. Phys.* **2016**, *16*, 5063–5073. [CrossRef]
69. Wang, S.-H.; Welton, E.J.; Holben, B.N.; Tsay, S.-C.; Lin, N.-H.; Giles, D.; Buntoung, S.; Chantara, S.; Wiriya, W.; Stewart, S.A.; et al. Vertical Distribution and Columnar Optical Properties of Springtime Biomass-Burning Aerosols over Northern Indochina during 2014 7-SEAS Campaign. *Aerosol Air Qual. Res.* **2015**, *15*, 2037–2050. [CrossRef]
70. Yin, S.; Wang, X.; Zhang, X.; Guo, M.; Miura, M.; Xiao, Y. Influence of biomass burning on local air pollution in mainland Southeast Asia from 2001 to 2016. *Environ. Pollut.* **2019**, *254*, 112949. [CrossRef]
71. Khan, R.; Kumar, K.R.; Zhao, T. The climatology of aerosol optical thickness and radiative effects in Southeast Asia from 18-years of ground-based observations. *Environ. Pollut.* **2019**, *254*, 113025. [CrossRef]

72. Krasnov, H.; Katra, I.; Koutrakis, P.; Friger, M.D. Contribution of dust storms to PM10 levels in an urban arid environment. *J. Air Waste Manag. Assoc.* **2014**, *64*, 89–94. [CrossRef]
73. Ogunjobi, K.O.; He, Z.; Simmer, C. Spectral aerosol optical properties from AERONET Sun-photometric measurements over West Africa. *Atmos. Res.* **2008**, *88*, 89–107. [CrossRef]
74. Falaiye, A.; Babatunde, E.; Willoughby, A. Atmospheric aerosol loading at Ilorin, a tropical station. *Afr. Rev. Phys.* **2015**, *9*, 527–535.
75. Chakraborty, A.; Bhattu, D.; Gupta, T.; Tripathi, S.N.; Canagaratna, M.R. Real-time measurements of ambient aerosols in a polluted Indian city: Sources, characteristics, and processing of organic aerosols during foggy and nonfoggy periods. *J. Geophys. Res. Atmos.* **2015**, *120*, 9006–9019. [CrossRef]
76. Chen, H.; Cheng, T.; Gu, X.; Li, Z.; Wu, Y. Characteristics of aerosols over Beijing and Kanpur derived from the AERONET dataset. *Atmos. Pollut. Res.* **2016**, *7*, 162–169. [CrossRef]
77. Joo, S.; Naghmeh, D.; Noh, Y. A Study on the Characteristic Variations of Fine Particle in Busan and Ulsan through Particle Extinction Efficiency Analysis. *J. Korean Soc. Atmos. Environ.* **2021**, *37*, 80–90. [CrossRef]
78. Uno, I.; Wang, Z.; Itahashi, S.; Yumimoto, K.; Yamamura, Y.; Yoshino, A.; Takami, A.; Hayasaki, M.; Kim, B.-G. Paradigm shift in aerosol chemical composition over regions downwind of China. *Sci. Rep.* **2020**, *10*, 1–11. [CrossRef] [PubMed]
79. Plaza, J.; Pujadas, M.; Gómez-Moreno, F.; Sánchez, M.; Artíñano, B. Mass size distributions of soluble sulfate, nitrate and ammonium in the Madrid urban aerosol. *Atmos. Environ.* **2011**, *45*, 4966–4976. [CrossRef]